RSC Publishing Soft Matter

Molecular Mechanisms of Phosphatidylcholine Monolayer Solidification due to Hydroxyl Radicals

Journal:	*Soft Matter*
Manuscript ID:	SM-ART-02-2011-005312.R1
Article Type:	Paper
Date Submitted by the Author:	n/a
Complete List of Authors:	Helm, Christiane; Ernst Moritz Arndt Universität, Institut für Physik Ahrens, Heiko; Universität Greifswald, Institut für Physik Ortmann, Thomas; Universität Greifswald, Institut für Physik Lawrenz, Frank; Universität Greifswald, Institut für Physik Brezesinski, Gerald; MPI Kolloid- und Grenzflächenforschung, Oberflächen Scholz, Fritz; Universität Greifswald, Institut für Biochemie

Molecular Mechanisms of Phosphatidylcholine Monolayer Solidification due to Hydroxyl Radicals

Andreas Gröning[1,2], Heiko Ahrens[1], Thomas Ortmann[1], Frank Lawrenz[1], Gerald Brezesinski[2], Fritz Scholz[3], Christiane A. Helm[1]

[1]*Institut für Physik, Ernst-Moritz-Arndt Universität, Felix-Hausdorff-Str. 6, D-17487 Greifswald, Germany*

[2]*MPI für Kolloid- und Grenzflächenforschung, D-14476 Potsdam, Germany*

[3]*Institut für Biochemie, Ernst-Moritz-Arndt Universität, Felix-Hausdorff-Str. 4, D-17487 Greifswald, Germany*

ABSTRACT

The reaction of L-α-1,2-dipalmitoylphosphatidylcholine (DPPC) with hydroxyl ($HO^{\bullet}$) radicals (Fenton solutions) was investigated using monolayer techniques: isotherms, infrared reflection absorption spectroscopy (IRRAS), gracing incidence X-ray diffraction, X-ray reflection and fluorescence microscopy. The DPPC monolayer is attacked with different $HO^{\bullet}$ concentrations. The decrease of the lateral pressure was used as a measure of the efficiency of the $HO^{\bullet}$ attack. With increasing $HO^{\bullet}$ concentration, the plateau region in the isotherm was shifted to a lower surface pressure; eventually it disappeared. Fluorescence microscopy during the $HO^{\bullet}$ attack showed that new domains in the condensed phase nucleate immediately. With isotherms and X-ray diffraction we found that the monolayer can be compressed to smaller molecular areas, with a reduced tilt angle of the alkyl chains. IRRAS experiments indicated a partial cleavage of the head group leading to a reduced head group size.

INTRODUCTION

Under aerobic conditions, biological systems are constantly exposed to reactive oxygen radicals (ROS) (a) because ROS are by-products of the normal metabolism, (b) because ROS are deliberately formed as reagents in the immune response systems, (c) because some ROS are messengers in biochemical systems. and (d) because ROS are constantly produced by irradiation (esp. UV) and also in chemical reactions involving transition metal ions (e.g., Fenton reaction, i.e. the reaction of H_2O_2 with Fe^{2+}).[1-2]

Deleted: [1]

ROS are known to play an important role in many pathological pathways, in cancer development, aging etc. Whereas the role of ROS in biochemical cycles has attracted much attention, the interaction of ROS with cell membranes, especially with their basic constituents –the lipids– still needs much more detailed studies, especially with respect to the biophysical consequences. One of the hallmark features of cellular life is the presence of membranes that separate the cell from the rest of the world and its compartments from each other. Hence it is easy to understand that membranes are also the first barriers with which ROS will interact when cells are exposed to these aggressive chemical species. Membranes are characterized by mechanical properties that demand an energy cost for bending them away from their equilibrium configuration. The elasticity of the membrane depends strongly on the composition of the membrane and the self-assembly of the different constituents. It is therefore very interesting to study how ROS affect the mechanical properties of membranes, esp. in the context of lipid peroxidation.[3]

Deleted: [2]

The primary constituent of any biological membranes are lipids, molecules consisting of hydrophobic alkyl chains (tails) bound to a hydrophilic head group. Certain features of lipid packing in membranes can be understood on the basis of the geometry of those molecules. Different species of lipids can have both different numbers of hydrophobic tails (the generic cellular case is two tails) and different tail lengths.

Lipid monolayers frequently serve as model systems to study the assembly, the phases and viscoelastic properties of different membranes. The effect of molecular shape is especially clear in the condensed phase, when the molecules are laterally compressed, and the fatty acid tails are in an all-trans conformation.[4-5] Then, the crystallographic phase of the tails is strongly influenced by the constraints imposed by the head group. Phosphatidylcholines (PC), which constitute 10-20 % of membranes have a large head group.

Knowing the cross section $A_0 = 20.2$ Å^2 per tail (for tilt angle $t = 0$),[5] the tilt angle is given by $A_0/A = \cos t$ under the assumption of constant density of the hydrophobic region (A is the known molecular area from the isotherm). Therefore, in the condensed phase of phosphocholines the tails are tilted by about 30° with respect to the membrane normal. In contrast, phosphatidylethanolamines (PE) or phosphatidic acids (PA) have a smaller headgroup; its area corresponds to the cross-section of the two alkyl chains in the all-trans conformation.[6] Therefore, for PA and PE the tails are oriented perpendicular to the membrane. Chemically, PC differs from PE by three methyl groups bound to the N-atoms in the headgroup. Removal of one or even two of these methyl groups reduces the headgroup size, which is evidenced by the reduced tilt angle in the condensed phase.[7]

On a thermodynamic level, the large head group of the PC causes a lateral intermolecular repulsion which needs to be overcome, if the lipids undergo the phase transition from the liquid into the condensed phase. Therefore, PC vesicles have a lower melting temperature than PE vesicles (provided they have the same number of C-atoms per chain[6]). In the same manner, one needs to compress PC monolayers to higher surface pressure to induce the fluid/condensed phase transition than PE or PA monolayers (for the latter, the electrostatic repulsion between the head groups needs to be screened by suitable counterions[4]).

Here we shall describe the results of experimental studies of the interaction of ROS with monolayers of L-α-1,2-dipalmitoylphosphatidylcholine (DPPC). This phosphocholine was chosen because its fluid and condensed phase are well characterized, both on thermodynamic

Deleted: [3]

Deleted: [4]

Deleted: [5]

Deleted: [4]

Deleted: [3a]

and a molecular level[4]. Specifically, we have generated $HO^{\bullet}$ radicals with the help of the Fenton reaction, which can be written in its most basic form as follows: $H_2O_2 + Fe^{2+} \longrightarrow OH^- + OH^{\bullet} + Fe^{3+}$. However, one must be aware of the fact that Fe^{3+} also reacts with H_2O_2 according to $H_2O_2 + Fe^{3+} \longrightarrow H^+ + HO_2^{\bullet} + Fe^{2+}$ and the formed hydroperoxyl radical will further react with H_2O_2 according to $H_2O_2 + HO_2^{\bullet} \longrightarrow O_2 + HO^{\bullet} + H_2O$.[8-9] This means that not only $HO^{\bullet}$ radicals, but at least also $HO_2^{\bullet}$ radicals are present in Fenton solutions. There were two reasons that prompted us to use Fenton solutions for the generation of $HO^{\bullet}$ radicals: Fenton solutions allow a rather reproducible formation of $HO^{\bullet}$ radicals, and the reaction has a special relevance because it proceeds practically everywhere where hydrogen peroxide and iron is present.

Thermodynamic data about the effect of ROS on the phase behaviour of DPPC monolayers are obtained with isotherms. Possible changes in the molecular composition are investigated with IRRAS (infrared reflection absorption spectroscopy). The in-plane order and its changes is monitored with Grazing Incidence X-ray diffraction. The electron density profile perpendicular to the water surface is measured with X-ray reflectivity. The coexistence region of the fluid and the condensed phase is imaged with fluorescence microscopy, to visualize the effect of ROS on the phase composition.

Deleted: [3a]

Deleted: [6]

MATERIALS AND METHODS

2.1. Materials

L-α-1,2-dipalmitoylphosphatidylcholine (DPPC) was purchased from Avanti Polar Lipids (Alabaster, AL) and used without further purification. The phospholipid is dissolved in chloroform. For fluorescence microscopy experiments, 0.25 mol% of 16:0-12:0 NBD PC (1-palmitoyl-2-{12-[(7-nitro-2-1,3-benzoxadiazol-4-yl)amino]dodecanoyl}-*sn*-glycero-3-phosphocholine, Avanti Polar Lipids, Alabaster, AL) was added. This is a fatty acid labelled fluorescent lipid. The Fenton reaction was used to generate hydroxyl radicals. Therefore the subphase was an aqueous solution consisting of Mohr's salt (ammonium iron sulphate, Merck, Darmstadt, Germany) and EDTA (ethylenediaminetetraacetic acid, Sigma-Aldrich-Chemie, Steinheim, Germany) in the ratio 4:5. The concentration of Mohr`s salt was varied between 0.5 to 5 mM. 1.5 M H_2O_2 (hydrogenperoxid, Merck, Darmstadt, Germany) solution was used in all experiments. The molar ratio between Fe^{2+} und H_2O_2 was set to 1:3, if not otherwise indicated. In the text, we refer to this aggressive mixture as Fenton solution.[10]

Deleted: [7]

Langmuir film balance and Fenton reaction

The lateral pressure/area isotherm of DPPC was recorded before and after $HO^{\bullet}$ attack on a film balance from Riegler & Kirstein (R & K, Potsdam, Germany). The area of the trough was 3.5 × 30 cm^2. The temperature was set to 21°C by a thermostat (DC-30 Thermo-Haake, Haake-Technik, Karlsruhe, Germany); and the lateral pressure was measured with a filter paper as Wilhelmy-plate. The subphase contained Mohr's salt and EDTA. After spreading the DPPC containing solution on the subphase, chloroform was allowed to evaporate for 10 minutes. The monolayer was compressed at a velocity between 3 and 9 $Å^2$ $molecule^{-1}$ min^{-1}. When the desired surface pressure was reached, for a $HO^{\bullet}$ attack the necessary amount H_2O_2

(1.5 M) was injected either by a pump (Reclo digital MS-4/8, ISMATEC, Wertheim-Mondfeld, Germany) or by a syringe into the subphase and stirred with caution. During the reaction the area per molecule was kept constant.

IRRA spectroscopy

IRRAS was measured using a film balances from R & K (Potsdam, Germany) and NIMA Technology (Coventry, Great Britain). The principle of the method and its application to Langmuir films at the air-water interface are described elsewhere.[11] The spectra were acquired with an IFS 66 FT-IR spectrometer from Bruker (Ettlingen, Germany), which is equipped with an external reflectance unit (XA – 511, Bruker) containing a Langmuir trough setup. The incidence angle is adjustable due to a computer-driven rotation of a mount, which contains a series of mirrors. These mirrors reflect the infrared beam of the spectrometer to the water surface. Before the IR – beam hits the water surface, a KRS-5 (thalium bromide and iodide mixed crystal) wire grid polarizer, is placed into the optical path. The reflected beam follows an equivalent mirror path and is registered at the same angle as the angle of incidence by a MCT (mercury–cadmium–telluride) detector, which is cooled with liquid nitrogen. To compensate residual water vapour rotation–vibration bands a Langmuir trough consisting of two parts was used.[11-12] One part was covered by the monolayer (sample), the other one is monolayer-free (reference). Both parts are connected to ensure the same surface height. A shuttle system moved alternately between the two parts to collect the interferograms of sample and reference. In all experiments, the FTIR spectra were collected at a resolution of 8 cm^{-1} using 200 scans for s-polarized light and an angle of incidence of 40°. The entire experimental setup was enclosed to keep the relative humidity constant. IRRA spectra are presented as absorbance vs. wavenumber. Absorbance, also reflectance–absorbance, is obtained from

Deleted: [8]

Deleted: [8-9]

$-\log(R/R_0)$, where R is the single-beam reflectance of the sample and R_0 the single-beam reflectance of the reference.[13-14]

Deleted: [10]

Fluorescence microscopy

Fluorescence microscopy was performed with a modified Zeiss Axiostar plus epifluorescence microscope (Zeiss, Jena, Germany). To eliminate scattering from the bottom of the R & K Langmuir trough, a piece of black glass was placed on the bottom, under the microscope objective. To prevent convection caused by air currents and to keep the Langmuir trough free from airborne impurities, the entire trough and microscope were enclosed in a plexiglas housing. To minimize monolayer movement, a small and flat cylinder with two openings opposite of each other (they allowed the monolayer to flow in and out) was attached in the Langmuir trough. For the objective (EC Epiplan 20 x / 0.4 or 50 x / 0.7 from Zeiss), there was furthermore one opening at the top of the cylinder. The fluorescence images were monitored with a CCD camera (Colorview II, Olympus, Münster Germany) and analysed with Cell F (Olympus Soft Imaging Solution GmbH).

Grazing incidence X-ray diffraction

Grazing-incidence diffraction measurements were performed at the liquid surface diffractometer at the undulator beam line BW1 in HASYLAB, DESY, Hamburg, Germany. The synchrotron beam is made monochromatic with a wavelength of λ = 1.303 Å by Bragg reflection from a beryllium (002) crystal.[15] This x-ray beam strikes the surface at grazing-incidence angle $\alpha_i = 0.85\ \alpha_c$, where $\alpha_c \approx 0.13°$ is the critical angle for total external reflection. To damp waves, the water height beneath the irradiated area was reduced to ca. 500 µm with a glass block. If the electron density on the surface is laterally periodical, the evanescent wave is dif-

Deleted: [11]

fracted, and one observes Bragg peaks. A linear position sensitive detector (Mythen, Paul-Scherrer Institut, Villingen, Switzerland) measured the intensity of the diffracted beam as a function of the out-of-plane (vertical) scattering angle α_f, i.e. the out-of-plane component $Q_z = 2\pi/\lambda \cdot \left(\sin\alpha_i + \sin\alpha_f\right)$ of the scattering vector $\boldsymbol{Q}$. A Soller collimator in front of the detector provides a horizontal resolution of $\Delta Q_{xy} = 0.0085$ Å^{-1}. The horizontal in-plane component of the scattering vector, $Q_{xy} = 2\pi/\lambda \cdot \sin(2\theta/2)$ is varied by rotating the entire detector arm (detector and Soller collimator) by the horizontal scattering angle 2θ. Q_z contains information about the tilt direction of lipid chains, whereas Q_{xy} provides information about the laterally periodic structure of the monolayer. The experimental setup and the data evaluation procedure are described in detail elsewhere.[15-16]

Deleted: [11-12]

X-ray reflectivity

The X-ray reflectivity of a monolayer at the air/water interface is a function of the perpendicular scattering vector $Q_z \approx 4\pi/\lambda \cdot \sin\alpha$, with $\alpha = \alpha_i = \alpha_f$. In the kinematic approximation, the reflectivity R is the interference pattern caused by the thin layer on top of the subphase[17] multiplied by the Fresnel reflectivity R_F obtained from an infinitely sharp interface.

Deleted: [13]

To calculate the electron density profile $\rho(z)$ of the thin layer on top of the subphase (with $\rho_{sub} \approx 0.334$ e Å^{-3} for water), one has to use models. A successful strategy is to represent the monolayer as a stack of slabs, each with a constant electron density ρ_i and thickness l_i. The model density is smeared at slab interfaces to account for the intrinsic vertical roughness or diffuseness of the interfaces. The roughness, σ, is on the order of 3 - 4 Å and stems mainly from thermally excited capillary waves on the water surface. To allow for multiple reflections, as well as absorption effects close to the critical angle, for the actual data fitting the exact Fresnel equations are used.[16] For a lipid monolayer the electron density profile is described by a model consisting of two slabs, one for the hydrophobic alkyl tails and the other for the po-

Deleted: [12]

lar, electron-rich head group. Since $\rho_{tail} \leq \rho_{sub}$ and $\rho_{head} > \rho_{sub}$, the position of the first minimum gives the length[18]: $l_{tail} + 1/2 l_{head} = 3\pi/(2Q_{z,min})$. X-ray reflectivity measurements were performed with a home-built setup.[19]

Deleted: [14]

Deleted: [15]

RESULTS

Isotherms and $HO^{\bullet}$ attack

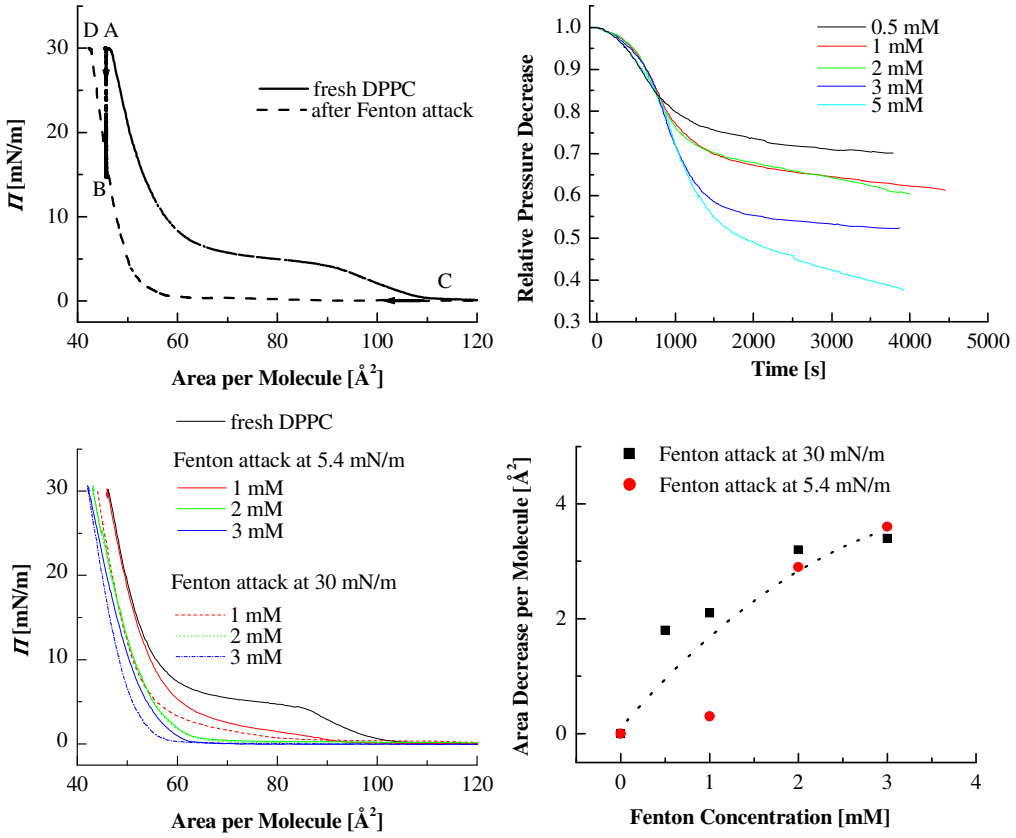

Figure 1. The effects of a $HO^{\bullet}$ attack on the DPPC isotherm at 21°C. "Fenton concentration" denominates the concentration of Mohr's salt with added EDTA and H_2O_2 in ratios given in the text. Top left: Isotherm prior to a 2 mM Fenton attack at 30 mN/m. While the molecular area was kept constant, the lateral pressure decreased during 3 hours. The subsequent decompression/compression demonstrated a decrease of the molecular area at 30 mN/m. Top right: The time resolved decay of the lateral pressure for $HO^{\bullet}$ attacks at Fenton concentrations indicated (attack at 30 mN/m). When the lateral pressure reached a new equilibrium value, the $HO^{\bullet}$ attack was considered finished. Bottom left: Compression isotherms after $HO^{\bullet}$ attacks at conditions indicated. Bottom right: Decrease of the molecular area at 30 mN/m versus the Fenton concentration. The DPPC monolayer was either attacked in the coexistence region or in the condensed phase, as indicated. The dotted line is a guide to the eye.

The lateral pressure/area isotherm of a DPPC monolayer on Mohr's salt and EDTA is shown in Fig. 1 (top, left). It is very similar to the isotherm of DPPC on pure water. Briefly, the monolayer undergoes a transition from a liquid-expanded to a condensed state characterized by a plateau region. The onset of the coexistence region occurred at π_c = 4.6 mN/m. To quantify the effects of a $HO^{\bullet}$ attack, (a) the Fenton concentration and (b) the phase state of the monolayer were varied (either the coexistence region at 5.4 mN/m or the liquid-condensed phase at 30 mN/m). During the $HO^{\bullet}$ attack, the molecular area was kept constant while the decrease of the surface pressure was monitored (cf. Fig. 1, top right). In both cases, the pressure decrease was for the first half hour independent of the actual Fenton concentration. For higher Fenton concentrations, the pressure decrease kept going on longer. Two or three hours after the $HO^{\bullet}$ attack, a new equilibrium value was reached. Then, the $HO^{\bullet}$ attack was considered finished.

After completion of the Fenton attack, a second isotherm was measured, which was identical to all subsequent isotherms. With increasing Fenton concentration, the plateau region shifted to a lower surface pressure; and it even disappeared when the Fenton concentration was 2 mM or larger (cf. Fig. 1, bottom left). When the fluid phase disappeared, the steep pressure increase typical for the condensed phase shifted to lower molecular areas. Furthermore, the monolayer could be compressed to a lower molecular area. At a selected surface pressure (i.e. 30 mN/m) the loss in molecular area was quantified. The area decrease grew monotonically with the Fenton concentration, at least up to 5 mM (cf. Fig. 1, bottom right). Experiments with higher Fenton concentration were impossible due to the high oxygen production, the oxygen bubbled up and destroyed the monolayer.

Fig. 1 (bottom) suggests that at a specific concentration the Fenton attack is more efficient when the monolayer is in the condensed phase (cf. shift of the transition pressure π_c, and decrease of the molecular area at 30 mN/m). Note that this is only a qualitative observation..

For the other experiments (IRRAS, X-ray diffraction and reflectivity, fluorescence microscopy) different troughs with a different area/volume ratio were used. Then, the efficiency of the $HO^{\bullet}$ attack and the kinetics of the monolayer rearrangement changed. To measure the efficiency of the $HO^{\bullet}$ attack we used the absolute pressure decrease. Always, we waited until a stable pressure was reached.

IRRA spectroscopy

A possible explanation for the decrease of the molecular area in the compressed monolayer is the fragmentation of DPPC, followed by the dissolution of the fragments.

An IRRA spectrum of a DPPC monolayer recorded at 21°C at a pressure of 30 mN/m is shown in Fig. 2. The spectral regions between 900 and 1800 cm^{-1} and 2800 and 3000 cm^{-1} are very important for obtaining information on the orientation and conformational order of hydrocarbon chains, on the subcell structure ($\nu_s(CH_2)$ and $\nu_{as}(CH_2)$), on the hydration, H-bonding, and ion binding (e.g., $\nu(CO)$, $\nu(PO_2^-)$), as well as on the conformation of the head group ($\nu(CN^+C)$, $\nu(PO_2^-)$).[13]

Deleted: [10a]

After a $HO^{\bullet}$ attack at 30 mN/m another IRRA spectrum was recorded at the same molecular area but at the new equilibrium pressure (13 mN/m). Then, the monolayer was recompressed to 30 mN/m, in order to compare the IRRA spectra at the same surface pressure.

Fig. 2 shows the IRRA spectra of DPPC before and after $HO^{\bullet}$ attack in a spectral range of 950 to 1300 cm^{-1}. The vibrations of CN^+C at 975 cm^{-1} and $R_1O\text{-}P\text{-}OR_2$ at 1061 cm^{-1} are characteristic for DPPC.[13,20] The intensity of $\nu_{as}(CN^+C)$ decreased after $HO^{\bullet}$ attack, which may be an indication for a partial cleavage of DPPC. But this band cannot be used for quantification because the response of the detector drastically decreases at wave numbers smaller than 970 cm^{-1}. Additionally the intensity of this band is quite weak, and the signal/noise radio decreases especially in this region due to evaporation of water during reaction time.[13]

Deleted: [10a, 16]

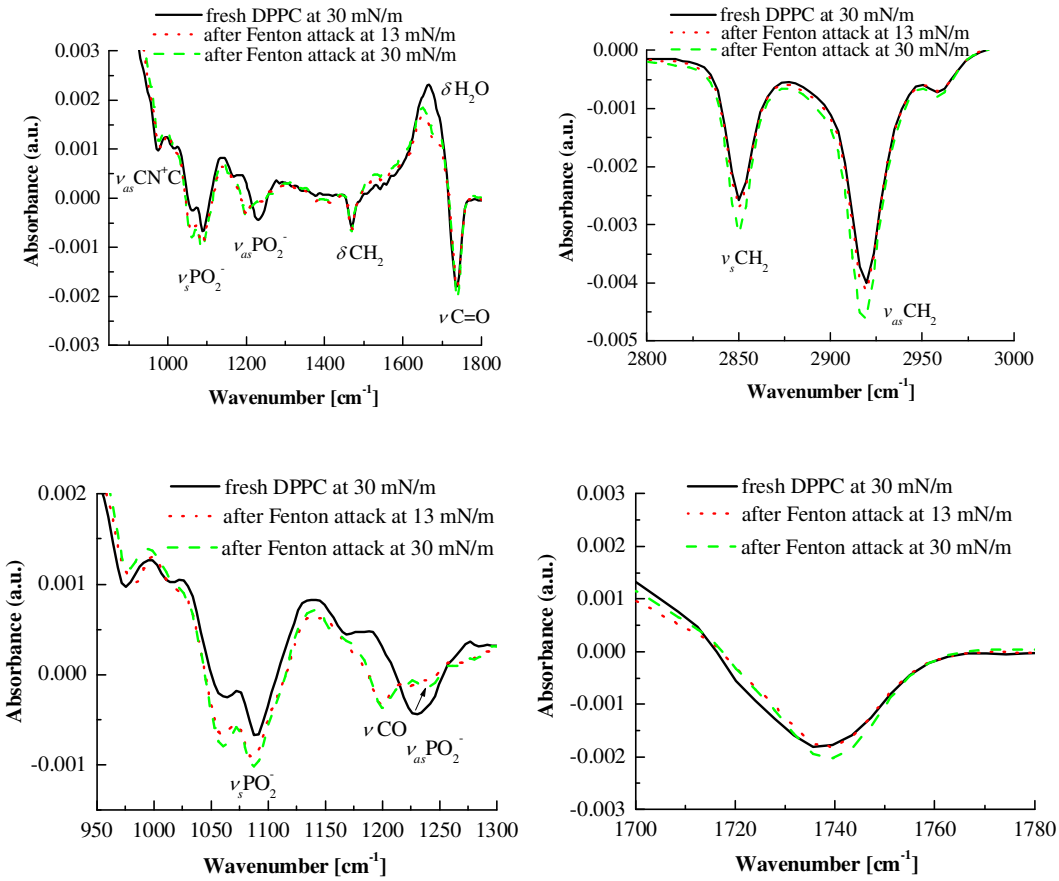

Figure 2. s-polarized IRRA spectra of a DPPC monolayer at 21°C before (30 mN/m, solid line) and after $HO^{\bullet}$ attack with a concentration of 2 mM**.** After the $HO^{\bullet}$ attack the pressure relaxed within 3 hours to a new equilibrium value of 13 mN/m (dotted line, red). The last spectrum was measured after the film was recompressed to 30 mN/m (dashed line, green). Top: Changes in the part of the spectrum characterized by bands attributed to the head group (left) and to the fatty acid chains (right). Bottom: Enlarged spectra of the vibration bands of the PO_2^- (left) and the CO (right) groups.

DPPC generated phosphate stretching vibrations at 1088 cm^{-1} ($\nu_s(PO_2^-)$) and at 1230 cm^{-1} ($\nu_{as}(PO_2^-)$) (cf. Fig. 2, left). The $HO^{\bullet}$ attack leads to an intensity increase of the symmetric $\nu_s(PO_2^-)$ and a decrease of the asymmetric $\nu_{as}(PO_2^-)$ phosphate vibrations. The $R_1O\text{-}P\text{-}OR_2$ band at 1061 cm^{-1} also increases in intensity. Obviously, the head group changed with respect to orientation and charge. DPPC is a zwitterionic molecule and the positions of the vibrational

Deleted: [10a]

bands do not change as a function of pH and ionic composition.[13] If the choline group or trimethylamine would be cleaved due to radical attack, the water soluble choline or trimethylamine dissolve and the head group of the remaining compound bears a single negative charge. In this case, different ionic composition and pH-values will affect the ionization degree and the orientation of the PO_2^- group with respect to the monolayer plane.[13] The observed isotherm is also in accordance with that of a mixed monolayer composed of the zwitterionic DPPC and an anionic lipid, as e.g. DPPA,[21] if the amount of the anionic lipid is more than 50 %. This amount is supported by the decreased intensity of the CN^+C stretching vibration. The shift of the asymmetric phosphate vibration can be explained by close association with Fe^{2+} ions. Normally the Fe^{2+} ions are bounded in an EDTA complex. But one can imagine that hydroxyl-radicals destroy the complex and some Fe^{2+} ions are released.[13]

Deleted: [10a]

Deleted: [10a]

Deleted: [17]

Deleted: [10a]

Scheme 1. Suggested reaction scheme of a hydroxyl-radical with a DPPC molecule within a lipid monolayer.

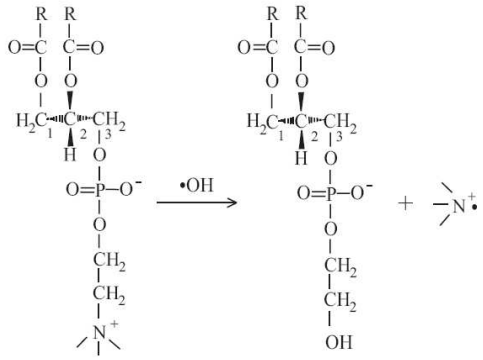

Interestingly, a new band was observed at 1200 cm^{-1} after $HO^\bullet$ attack. This band can be attributed to a CO single bond stretching vibration and may be explained as the result of the cleavage of trimetylamine due to the reaction with a hydroxyl-radical (cf. Scheme 1). Thereby

a new $N(CH_3)_3$-radical is formed, which can react further, for instance with another hydroxyl-radical to trimetylaminoxid.

Furthermore, Fig. 2 (bottom right) shows the region of the ester stretching vibrations ν(C=O). This band consists of two overlapping components, one at 1740 cm^{-1} and another at 1726 cm^{-1}. The high-frequency component of this band is assigned to the non-hydrogen-bonded (free) carbonyl group, whereas the lower-frequency component can be taken as a proof for hydrogen-bonded carbonyl groups. After the $HO^{\bullet}$ attack, the band is more symmetric and a slight high-frequency shift as well as an increase of the intensity of the overall ν(C=O) band is observed (cf. Fig. 2). This can be explained by a tighter packing of the product after $HO^{\bullet}$ attack which additionally leads to a reduction of the hydrogen-bonded carbonyl group.[13]

Deleted: [10a]

Summarizing, IRRAS suggests a partial fragmentation of the DPPC head group. A decreased area requirement of the head group allows for a reduced tilt angle of the chains, as observed for condensed DPPA or DPPE. The positions of the CH_2 stretching bands at 2850 and 2918 cm^{-1} for the symmetric and asymmetric stretching vibrations, respectively, clearly indicated well-packed alkyl chains with all-trans conformation in the recompressed monolayer after the Fenton attack. Actually, the intensity of the bands in the spectral region between 2800 and 3000 cm^{-1} increased, which is consistent with a lower tilt angle (changed orientation) and a higher packing density. For quantification of the alkyl chain order in the liquid-condensed phase, X-ray diffraction measurements were performed.

Grazing incidence X-ray diffraction

The crystalline structure of the alkyl tails before and after the attack was recorded. The left column in Fig. 3 shows diffraction peaks obtained from a freshly prepared DPPC monolayer at the end of the coexistence region (on a solution containing 2 mM Mohr's salt, and 2.5 mM EDTA), in qualitative agreement with earlier observations.[5] Two peaks can be clearly distinguished: the first at $Q_{xy} \approx 1.45$ Å^{-1} ($Q_z = 0$) and the second (degenerated) peak at $Q_{xy} \approx 1.28$ Å^{-1} and $Q_z \approx 0.75$ Å^{-1}. These peaks are typical for a tilt of the alkyl chains in Next-Neighbor (NN) direction. The structure was fitted by seven parameters: two Q_{xy} positions (defining the 2-dimensional lattice), two different peak widths in Q_{xy} direction (inversely proportional to the correlation length of the 2-dimensional order), one Q_z position (measure of the tilt of the alkyl chains), one peak width in Q_z-direction (inversely proportional to the alkyl chain length) and two peak intensities.

On monolayer compression the Q_{xy}-positions of the peaks shifted to larger values, indicating a decrease of the lattice dimensions. Simultaneously, the peak position at large Q_z-values decreased, showing a decrease of the tilt angle. On a closer look, the principal axis of the high Q_z-peak was inclined to the Q_z-axis and the peak was broadened on compression, resulting in continuous banana shaped intensity distribution for the highest pressure measurement. To model the peak distortion we assumed as an additional parameter a distribution of the tilt azimuth direction $\Delta\Psi$, i.e. we assumed an incoherent superposition from radiation diffracted at similar but slightly different 2-dimensional crystals.[16] The local arrangement of the alkyl chains perpendicular to the chain axis as well as the tilt angle are identical in all crystals. However, only few crystals show the exact NN-orientation, the tilt azimuth direction Ψ varies slightly between the crystals resulting in different lattice parameters in the surface plane. With this eight parameter model all diffraction data could be fitted (after the $HO^{\bullet}$ attack, for the measurement at 31.7 mN/m only one Q_{xy} peak width was used).

Deleted: [3b]

Deleted: [12]

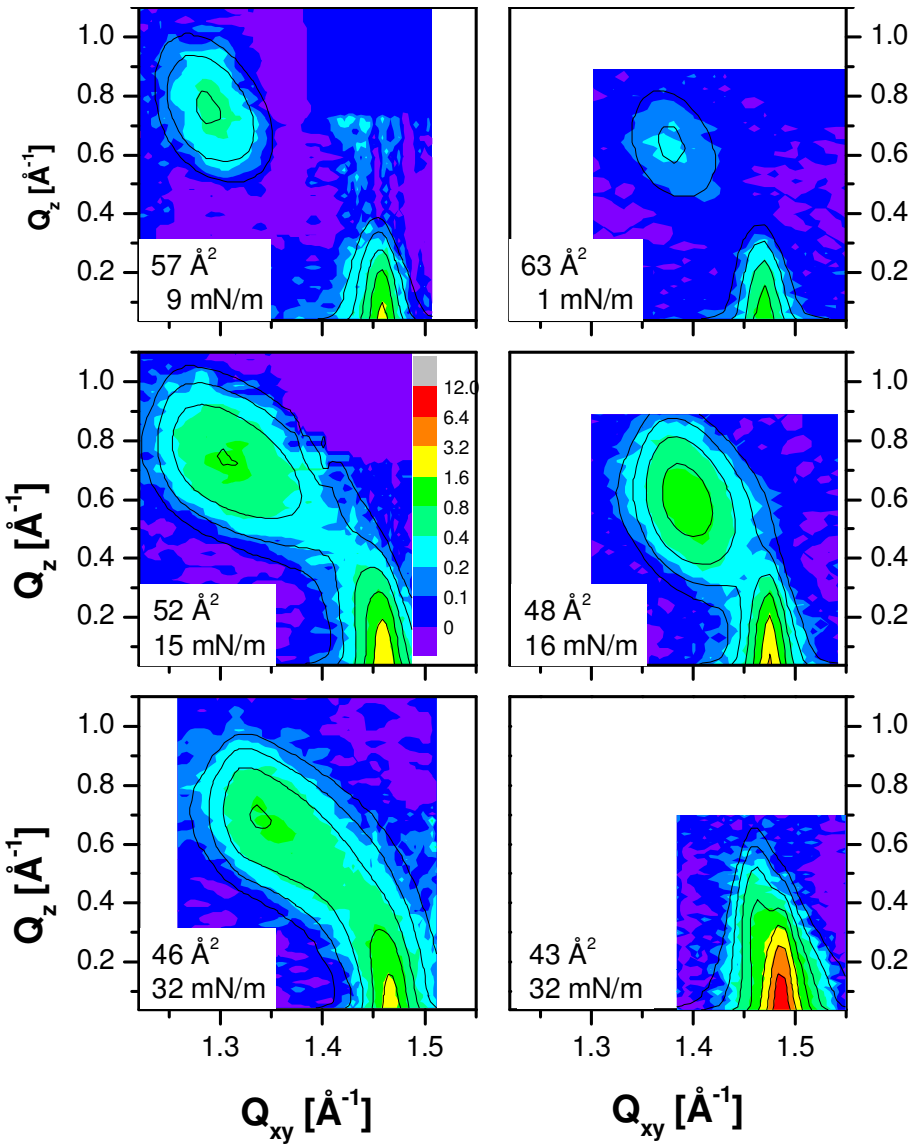

Figure 3. Grazing incidence X-ray diffraction measurements of a DPPC monolayer on a 2 mM Fenton solution, before and after the $HO^{\bullet}$ attack (details see text). The measurements are taken along the isotherm (top to bottom, lateral pressure and molecular area are indicated). Left: The fresh DPPC monolayer was characterized by two diffraction peaks, on compression the peak positions shifted to larger Q_{xy}-values indicating smaller lattice spacing. Simultaneously, the peak at large Q_z-positions moved to smaller values, a sign of a decreased tilt angle. Right: Monolayer compression after the $HO^{\bullet}$ attack: Already at almost zero lateral pressure (top), the out-of-plane peak occurred at larger Q_{xy}- and lower Q_z-positons. The lines are fits, the intensity is colour coded (note the almost logarithmic colour coding).

Two different monolayers were subject to a $HO^{\bullet}$ attack, one with the same amount of H_2O_2 as before, the other with an increased Fe^{2+} to H_2O_2 ratio (1:5). In the first case, the isotherm changed a little, similar to an attack at 1 mM and 5.4 mN/m, as depicted in Fig. 1 (bottom, left). After the strong $HO^{\bullet}$ attack, two diffraction peaks were already observed at zero pressure. These peaks (cf. Fig. 3, right) were qualitatively similar to those of the fresh DPPC monolayer, consistent with a tilt towards the next neighbor. However, already at very low pressure, the Q_z position of the second (degenerated) peak was decreased, indicating a decreased tilt angle. On compression, the peak moved towards lower Q_z, until the two peaks almost merged. Furthermore, after the attack the first peak (at Q_z=0) was more narrow in Q_{xy}-direction than before the attack, suggesting an increased correlation length within the surface plane.

Fig. 4 presents structural information deduced from the diffraction data. The tilt angle of the freshly prepared DPPC monolayer decreased on compression from 35° to 27° (cf. Fig. 4, top), consistent with earlier observations.[7] The large tilt angle of DPPC is necessary to accommodate the almost incompressible spacious head group. Assuming a constant alkyl chain density, the tilt angle t changes on decrease of the molecular area A as $\cos t = 40.4\ \text{Å}^2 / A$.[5] After the weak $HO^{\bullet}$ attack, the isotherm was almost the same, and so was the tilt angle. However, after the strong $HO^{\bullet}$ attack, the tilt angle was 30° at zero pressure. The decrease of molecular area at high pressures found with the isotherm (cf. Fig. 1) is accompanied by a reduced tilt angle, the minimum angle found was 15°. Such low tilt angles were observed for phospholipids with small head groups, PE or simple PA, or mixtures of zwitterionic PC with anionic PA.[5, Estrela-Lopis, 2004 #1006] Note that the measurement with the low tilt angle (π = 32 mN/m, cf. Fig. 3 right) had a large peak intensity, it exceeded all other measurements by an order of magnitude, suggesting pronounced condensation.

Deleted: [5]

Deleted: [3b, Estrela-Lopis, 2004 #1006]

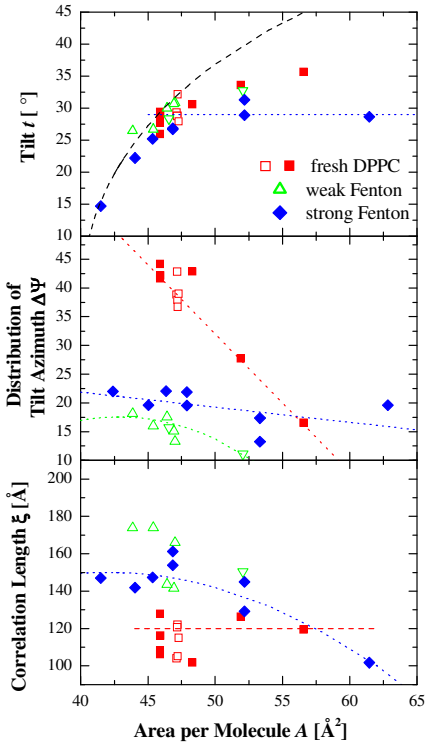

Fig. 4. Structural parameters deduced from the X-ray diffraction peaks measured along the isotherm. Two freshly prepared monolayers were analysed (red open and full squares). Also, two monolayers were attacked by $HO^{\bullet}$ and characterized afterwards, one attack was weak (green open triangles), and one strong (full blue diamonds). Top: tilt angle t with respect to the surface normal. After the strong $HO^{\bullet}$ attack, smaller molecular areas can be reached, they are accompanied by smaller tilt angles. Dashed line: tilt angle calculated with $\cos t = 40.4\ \text{Å}^2 / A$; dotted line: almost constant tilt angle in the condensed/gaseous coexistence region at 0 – 5 mN/m. Centre: Tilt azimuth distribution $\Delta\Psi$. On compression of the freshly prepared monolayers, $\Delta\Psi$ increased. After the $HO^{\bullet}$ attack, the tilt azimuth angle distribution was smaller. Dotted lines connect points obtained from the same films. Bottom: Correlation length ξ determined from the peak at low Q_{xy}. For the fresh monolayer, ξ was constant (ca. 120 Å, dashed line), after the $HO^{\bullet}$ attack it increased on compression to larger values, as illustrated by the dotted line.

Unexpected are the results concerning the tilt azimuth distribution $\Delta\Psi$ (cf. Fig. 4, centre). For the freshly prepared monolayer, $\Delta\Psi$ was low, and increased on monolayer compression

(from 15 to 45°). Clearly, the tail lattice was subjected to additional strain. Obviously, if the subphase contained EDTA and Mohr's salt, some molecules adsorbed tightly to the head group and changed the local conformation. Both for the weak and the strong $HO^{\bullet}$ attack, $\Delta\Psi$ was low and remained so on compression (15 to 20°), similar to DPPC on pure water. Presumably, the adsorbed molecules were destroyed during the $HO^{\bullet}$ attack, leading to a more stress-free alkyl tail lattice. The finding that the large azimuth angle distribution already disappears when the isotherm is only little changed indicates that the lateral interaction of the adsorbed species is weak.

The decreased peak width after the $HO^{\bullet}$ attack (cf. Fig. 3, right) suggests an increased correlation length. Shown are the correlation lengths in the surface plane perpendicular to the azimuth direction (cf. Fig. 4, bottom). For the freshly prepared monolayer, the correlation length was about 110 Å, and constant on compression. This value is lower than for a DPPC on pure water, where about 140 Å was observed which increased on compression to 180 Å. After the $HO^{\bullet}$ attacks, the correlation length increased on compression up to 140 – 160 Å (data not shown).

Deleted: [3b]

X-ray reflectivity

For X-ray reflectivity measurements, the DPPC monolayer on a 2 mM Fenton solution was compressed to 23 ± 1 mN/m (cf Fig. 5). After determining the X-ray reflectivity of the freshly prepared monolayer, the $HO^{\bullet}$ attack was performed. In this trough, the pressure decreased about 4 hours, until the new low equilibrium value was reached (8 mN/m). Two X-ray reflectivity measurements were taken (4.5 hours each), one during the monolayer reaction, the other, when the monolayer was in its new equilibrium state. After the X-ray reflectivity measurements, another compression isotherm was measured. The area decrease at 30 mN/m was about 4 – 5 $Å^2$/molecule, suggesting a very strong Fenton attack (cf. Fig. 1, bottom right).

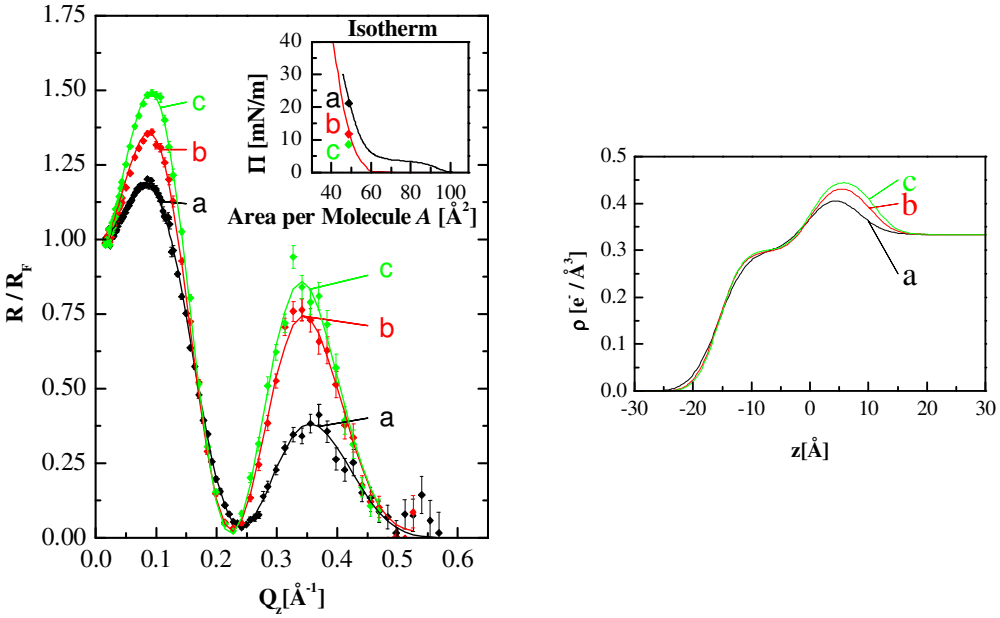

Figure 5. X-ray reflectivity normalized to the Fresnel reflectivity (left) and corresponding electron density profiles (right) of a DPPC monolayer on a 2 mM Fenton solution, before (measurement at 23 mN/m, black), during (b, red) and after (c at 8 mN/m, green) the $HO^{\bullet}$ attack. The molecular area was kept constant during the measurements. The isotherm is shown in the inset, with the surface pressure at which each reflectivity curve was measured indicated. Also shown is a compression isotherm after completion of the Fenton attack (red). Right: The electron density profiles indicate an unchanged hydrophobic region, while the head group increased in length and electron density. $z = 0$ is set at the interface between the hydrophobic and head group region.

The reflectivity measurements are rather typical for a phospholipid monolayer: The reflected intensity increased with Q_z until a maximum is reached. Then a minimum occurred; from the position of the minimum, the thickness of the monolayer was estimated. Additionally, a second well-defined maximum was observed.

After the $HO^{\bullet}$ attack, the intensity of the maxima was increased. The effect was already clear after two hours of pressure decrease, and got even more pronounced for the equilibrium measurement. Also, the positions of the minimum and the second maximum were shifted to lower Q_z-values, indicating film thickening.

For data analysis, the simple two-slab model for phospholipid monolayers was sufficient to describe the data, with a slab with low electron density for the hydrophobic group, and a slab with higher electron density next to the subphase for the head group. For a simple DPPC monolayer, the increased electron density in the latter is due to the electron-rich phosphate group.[7,22] However, the reflectivity data on Mohr's salt and EDTA solution are slightly different from DPPC on fresh water,[19,22] the first maximum is lower and a third maximum cannot be resolved. The data analysis showed that the DPPC head group on the Fenton solution (before the attack) is shorter than on fresh water.

Deleted: [5, 18]

The apparent shortening of the head group is caused by the adsorbed hydrated ions, i.e. EDTA. Note that the trimethylammonium group is almost invisible for X-ray reflectivity, since its electron density is very similar to H_2O. The same is true for the $-(CH_2)_2-$ group which binds the trimethylammonium group to the electron rich phosphate group. Obviously, the electron density of the adsorbed complexes is very similar to water, therefore one does not observe it directly, one can only monitor the consequences. Another indirect indication of an adsorbed layer before the radical attack was supplied by the X-ray diffraction data, there a low correlation length of the ordered alkyl chains and an unusual tilt azimuth distribution were observed.

After the $HO^{\bullet}$ attack at constant molecular area, the thickness and electron density of the hydrophobic tail group remained unchanged. This observation correlates well with the IRRA spectra which found that the chemical changes occur in the head group region, while the alkyl chains remain unaffected. According to X-ray reflectivity, the head group increased in length and electron density, suggesting Fe^{2+}-binding. We know that Fe^{2+} does not bind to a DPPC monolayer (X-ray reflectivity measurements of a DPPC monolayer on 2 mM of Mohr's salt solution with and without 2.5 mM EDTA were identical).

To quantify the apparent changes of the head group, one has to consider not only the electrons attributed of the DPPC head group, but also the incorporated H_2O molecules. An increased

head group volume can be the result of an increased hydration – this leads to a decreased electron density, although the number of electrons increases with the added water molecules. With the aim to compare the electrons E_{head} before and after the attack, we work with a constant volume of the head group, V_{head}. Therefore, the volume δV of water is added to head group until its maximum length l_{max} =11Å is reached. Then $V_{head} = V_{mol}+n_{H2O}\times V_{H2O}= A\times l_{max}$, with A the area per molecule (V_{mol} is the molecular volume of the DPPC head group without water). Similarly, the number of electrons in the head group needs to be adjusted $\delta E = \rho_{sub}\times\delta V = \rho_{sub}\times A\times(l_{max}-l_{head})$ (with ρ_{sub} the electron density of the subphase). This leads to $E_{head} = A\times(\rho_{head}\times l_{head} + \rho_{sub}\times(l_{max}-l_{head}))$.

Now, the number of electrons in the head group before $E_{head}(b)$ and after $E_{head}(a)$ the Fenton attack are compared, to calculate the change: $\Delta E = E_{head}(a) - E_{head}(b) = 20 - 25\ e^-$ which is comparable to one Fe^{2+} ion per DPPC molecule.

Considering the fact, that a Fe^{2+} ion has 24 electrons, one can assume that one Fe^{2+} binds per former DPPC molecule. Note that this conclusion is only valid if we assume that the PO_4-group with its large electron density remained in the head group. The other assumption is that the removed head group fractions have the same electron density as water (good approximation for the trimethylammounium and the CH_2 - groups) and the partial volume of Fe^{2+} is 0 (actually, it is negative [23]).

These assumptions about the head group after the attack are supported by the IRRA spectra. They suggested that the positively charged amine group was removed (cf. scheme 1), while the negatively charged phosphate group remained. However, one has to remember that the Fenton reaction does not only cleave the lipid head groups but also EDTA molecules. Therefore, Fe^{2+}-ions are liberated and can adsorb to the oppositely charged monolayer.

Fluorescence microscopy

The monolayer contained a NBD-DPPC fluorescent probe which was excluded from the solid phase, hence the domains are black, as an image at the end of the coexistence region shows (cf. Fig. 6). The domains were chiral (the mirror images cannot be superimposed), a result of the fact that L-α-DPPC itself is chiral.[4] The predominant domain shape was reminiscent of a bean, but multilobed shapes could also be observed.

Deleted: [3a]

During and directly after the $HO^{\bullet}$ attack, the monolayer was subject to percolation and pronounced drifts. Therefore, the first image was taken 2 min after the attack (cf. Fig. 6). Then, many more small domains did form. Actually, the size distribution of the domains was bimodal, suggesting sudden and homogeneous domain nucleation. The sudden pressure decrease caused by the $HO^{\bullet}$ attack was accompanied by a homogeneous nucleation. However, the lateral distribution of the domains was not homogeneous. Sometimes, the large domains touched. In some of these cases, a patch of the fluid phase was trapped between the large domains in the condensed phase. Then, the fluid phase showed an increased fluorescence intensity, due to the locally enriched dye concentration. These bright spots were often observed after a few minutes (cf. Fig. 6, image after 3 min). They occurred only between merged domains. Obviously, the sudden coalescence of the condensed domains did not allow the dye-labeld lipids NBD-DPPC to reach their equilibrium concentration in the fluid phase. The merging of the domains is likely to be caused by the monolayer movement accompanied by the $HO^{\bullet}$ attack.

After a few minutes, the large domains appeared to grow into all directions, reminiscent of the diffusion limited growth observed for PE monolayers on sudden compression.[24] After about 5 min, nothing can be seen anymore, because also the dye was attacked by the radicals. Actually, an increase in the Fenton concentration accelerated the bleaching of the dye. The chromophoric group inserts itself into the hydrophilic moiety even though it is bound to the alkyl

Deleted: [19]

chains,[25] therefore dye bleaching is to be expected if the hydrophilic region is the preferred zone of the chemical reactions.

Deleted: [20]

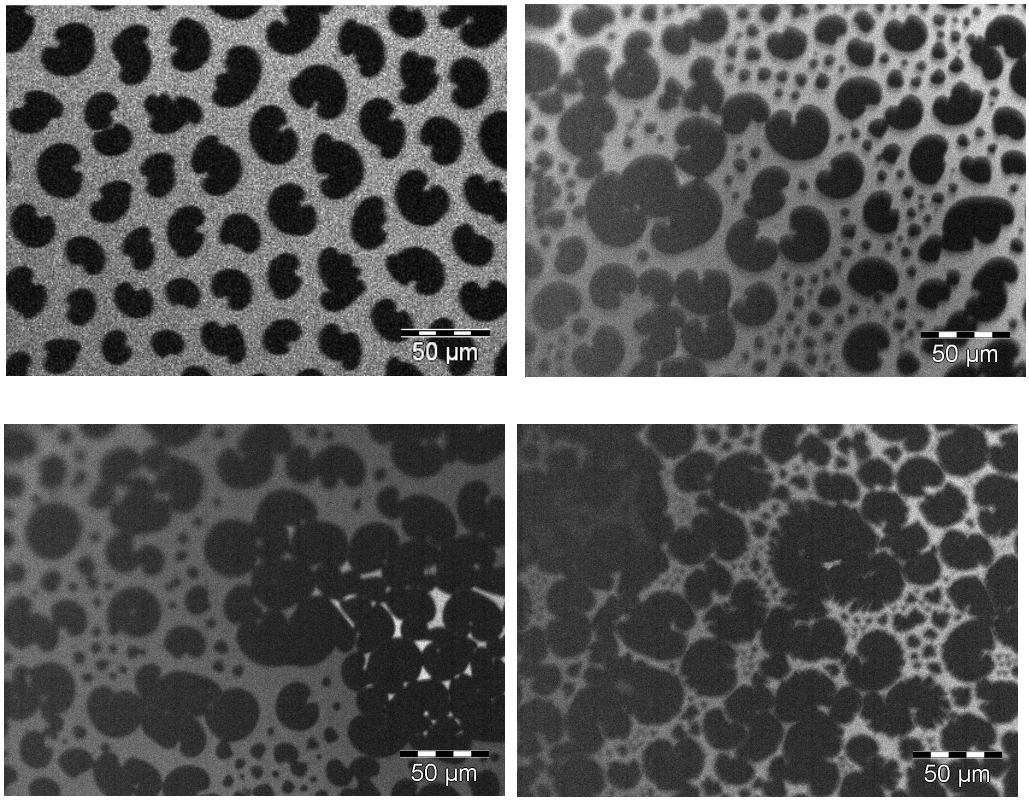

Figure 6. Fluorescence microscopy on a DPPC monolayer on a 2 mM Fenton solution, before and after the $HO^{\bullet}$ attack. Top left: The freshly prepared monolayer at 9 mN/m, in the coexistence region. The other images correspond two minutes (top right), 3 (bottom left) and 4 min (bottom right) after the $HO^{\bullet}$ attack. While the images were taken, the lateral pressure decreased (cf. Fig. 1) and the monolayer was subject to pronounced drifts. The scale bar corresponds to 50µm.

DISCUSSION

The changes of the isotherm due to a $HO^{\bullet}$ attack could be reproduced. A procedure to measure the efficiency of a $HO^{\bullet}$ attack was established: The decrease of the lateral pressure at a given molecular area was taken as a measure for the efficiency of the $HO^{\bullet}$ attack, not the concentration of Mohr's salt, the amount of EDTA and/or H_2O_2.

In different troughs with varying area/volume ratios, the efficiency of the $HO^{\bullet}$ attack was different. The life time of the radical oxygen species is very short, below seconds.[8] However, the slow pressure decrease observed at constant molecular area shows that it took the monolayer hours to rearrange. We do not know in detail which reactions occurred. We can only identify the monolayer region where most reactions took place – the head group region, specifically the cleavage of the trimethylammine group.

Deleted: [6a]

The different kinetics observed with different troughs may be caused by the following facts: (1) the H_2O_2 is injected locally with a syringe or a pump, (2) the Fenton reaction is fast, and (3) probably partly finished even before the stirring is completed. Therefore, how many radicals reach the monolayer surface does depend on depth and surface area of the trough, as well as the position of radical source. Therefore, the efficiency of the Fenton reaction changes from trough to trough.

Furthermore, not only the monolayer undergoes structural changes, but also Fe^{2+} originally bound to EDTA is liberated by the radical attack. Therefore, after the attack, an uneven distribution of Fe^{2+} is to be expected. Free Fe^{2+} has to diffuse to the charged head groups and bind to them. Any equation to describe the diffusion from a badly defined source to a flat surface is by necessity an approximation. In an attempt to understand the long time constants, we make assumptions: homogeneous distribution of the Fe^{2+} of unknown concentration; each Fe^{2+} which reaches the surface, sticks.[26] With a typical diffusion constant $D_{Fe2+} = 10^{-9}$ m^2 s^{-1}, a surface coverage of $\Gamma = 2 \times 10^{-18}$ nm^2, and a diffusion time of $t = 1000$ s, we obtain with the

Deleted: [21]

equation $\Gamma = 2c_o\sqrt{D_{Fe^{2+}}t/\pi}$ a concentration c_o = 3 µM. This is very low, indicating that the assumptions are not very good (presumably: the assumption of a homogeneous Fe^{2+} distribution is especially bad), however the idea that the long time scales observed are determined by bulk diffusion gains support..

After the new equilibrium surface pressure was reached, the monolayer could be compressed to a lower molecular area. The decreased molecular area is accompanied with less tilted alkyl chains than those observed for DPPC.[5-6] The minimum molecular area corresponding to 0° tilt angle is 40.4 Å^2.[5] Indeed, monolayers of PA or PE can be compressed to 0° tilt angles, since there is no mismatch between the molecular area of head group and of the two alkyl chains. Therefore, the decreased tilt angle and the decreased molecular area which can be achieved after attack are consistent with partial head group cleavage.

Deleted: [3b, 4]

Deleted: [3b]

For the freshly prepared monolayer, we found a large tilt azimuth $\Delta\Psi$ and a small correlation length. Therefore, some hydrated molecules (possibly EDTA) adsorbed to the zwitterionic DPPC monolayer, and locally influenced the head group arrangement. Only subtle changes of the diffraction data were observed (increased tilt azimuth distribution, decreased correlation length), which suggest a slightly different arrangement of the choline groups within the DPPC monolayer. Because one did not observe clear changes of the isotherm, nor a shift in the transition pressure π_c, nor a deviation of the IRRA spectra from DPPC on pure water, the adsorbed layers bound weakly, and did not affect lateral interactions in a perceptible way.

The preferential attack on the head group is not something to be expected. HO$^\bullet$ radicals could also easily enter the layer and damage the chains. HO$^\bullet$ radicals are not charged and so they could – in principle – easily partition and enter the monolayer. However, the data demonstrated a preferential attack of the head groups. IRRA spectra indicated head group cleavage, resulting in a negatively charged monolayer. There is strong evidence for the removal of the trimethylamine. The negative charge allowed electrostatic binding of Fe^{2+} ions, as evi-

denced by X-ray reflectivity. Actually, the alkyl tails were intact enough to form a lattice with a correlation length typical for DPPC on pure water. Yet the alkyl chains could be compressed to much lower tilt angles, since the head groups had a diminished size. Fluorescence microscopy showed that immediately after the $HO^{\bullet}$ attack domains nucleated homogeneously. All these findings demonstrate that the alkyl chains could form the condensed phase. They were in all-trans conformation and well packed (low wavenumbers of the CH_2 stretching vibrations), and they were not hindered by fragmentation or lateral polymerization.

We cannot exclude that an alkyl chain was cut off from the head group. Yet, if that happened, the alkyl chain remained in the hydrophobic moiety of the monolayer, as measurements of DPPC monolayers in an air atmosphere saturated with alkane showed.[27-28]

Deleted: [22]

The changed head group size affected the inter- and intramolecular interactions and therefore the thermodynamics of the monolayer. After the radical attack, we observed a decrease of π_c, suggesting decreased intermolecular repulsion. Actually, the transition pressure suggests an intermolecular interaction akin to PA or PE with their small head groups.[6]

Deleted: [4]

CONCLUSION

The DPPC monolayer was attacked with different Fenton concentrations. The decrease of the lateral pressure was used as a measure of the efficiency of the $HO^{\bullet}$ attack. With increasing Fenton concentration, the plateau region in the isotherm was shifted to a lower surface pressure; and disappeared eventually. Fluorescence microscopy during the $HO^{\bullet}$ attack showed that new domains in the condensed phase nucleate immediately after the attack. X-ray reflectivity suggests that after the attack Fe^{2+} binds to the monolayer, suggesting a net negative charge after the attack. Furthermore, isotherms demonstrated that the minimum molecular area attainable in the liquid-condensed phase was decreased. X-ray diffraction showed that at

this minimum molecular area the alkyl chains had a lower tilt angle than sterically possible for the large DPPC head group. IRRAS experiments indicated a cleavage of the head group. We conclude that a reduced head group size made a reduced tilt angle and a better order of the alkyl tails possible.

We attribute the solidification we observe to a preferential radical attack in the hydrophilic region of the monolayer. Summarizing, the subtle interplay of inter- and intramolecular interactions lead to the following effects: (i) immediate formation of condensed phase on $HO^{\bullet}$ attack, (ii) improved crystalline order in the condensed phase, (iii) lower molecular areas feasible, and (iv) a decreased intermolecular repulsion which reduces the phase transition pressure from the fluid to the condensed phase. The implications of the observed solidification of the monolayer for biological systems and membranes will be addressed in future collaborative research with scientists from biology and medicine.

ACKNOWLEDGEMENT

Financial support of the Graduate School “Studies of the interaction of free oxygen radicals with molecules at electrodes and applications to biochemical and medical systems” of the Alfried Krupp Wissenschafts Kolleg Greifswald and the Deutsche Forschungsgemeinschaft (He 1616/14-1) is appreciated. We thank HASYLAB at DESY, Hamburg, for beam time and for providing all necessary facilities. Stephan Block and Hans-Joachim Schmidt contributed a lot , when the fluorescence microscope was set up.

LITERATURE

(1) Jacob, C.; Winyard, P. G. *Redox signalling and regulation in biology and medicine*; Wiley-VCH: Weinheim, 2009.

(2) Ishimura, Y.; Nozaki, M.; Yamamoto, S.; Shimizu, T.; Narumiya, S.; Mitani, F. . In *Oxygen and Life: Oxygenases, Oxydases and Lipid Mediators. Excerpta Medica. International Congress Series 1233*; Elsevier: Amsterdam, 2002.

(3) vanGinkel, G.; Sevanian, A. Lipid peroxidation-induced membrane structural alterations. In *Oxygen Radicals in Biological Systems, Pt. C*; Packer, L., Ed.; Academic Press: San Diego, 1994; Vol. 233; pp 273.

(4) Möhwald, H. *Rep. Prog. Phys.* **1993**, *56*, 653.

(5) Kaganer, V. M.; Möhwald, H.; Dutta, P. *Reviews of Modern Physics* **1999**, *71*, 779.

(6) Cevc, G.; Marsh, D. *Phospholipid Bilayers: Physical Principles and Models*; John Wiley & Sons: New York, 1987; Vol. 5.

(7) Dyck, M.; Krüger, P.; Lösche, M. *PCCP* **2005**, *7*, 150.

(8) Lin, S.-S.; Gurol, M. D. *Environ. Sci. Technol.* **1998**, *32*, 1417.

(9) Walling, C. *Acc. Chem. Res.* **1975**, *8*, 125.

(10) Cortez, S.; Teixeira, P.; Oliveira, R.; Mota, M. *Journal of Environmental Management* **2010**, *92*, 749.

(11) Mendelsohn, R.; Brauner, J. W.; Gericke, A. *Annu. ReV. Phys. Chem.* **1995**, *46*, 305.

(12) Flach, C. R.; Brauner, J. W.; Taylor, J. W.; Baldwin, R. C.; Mendelsohn, R. *Biophys. J.* **1994**, *67*, 402.

(13) Estralda-Lopis, I.; Brezesinski, G.; Möhwald, H. *Biophys. J.* **2001**, *80*, 749.

(14) Wagner, K.; Desbat, B.; Brezesinski, G. *BBA - Biomembranes* **2008**, *1778*, 166.

(15) Jacquemain, D.; Wolf, S. G.; Leveiller, F.; Deutsch, M.; Kjaer, K.; Als-Nielsen, J.; Lahav, M.; Leiserowitz, L. *Angew. Chem. Int. Ed. Engl.* **1992**, *31*, 130.

(16) Günther, J.-U.; Ahrens, H.; Helm, C. A. *Langmuir* **2009**, *25*, 1500.

(17) Als-Nielsen, J.; Möhwald, H. Synchrotron x-ray scattering studies of Langmuir films. In *Handbook of Synchrotron Radiation*; Ebashi, S., Rubenstein, E., Koch, M., Eds.; North Holland, 1989; Vol. 5; pp 1.

(18) Kjaer, K. *Physica B* **1994**, *198*, 100.

(19) Baltes, H.; Schwendler, M.; Helm, C. A.; Möhwald, H. *J. Colloid and Interface Science* **1996**, *178*, 135.

(20) Wagner, K.; Brezesinski, G. *Biophys. J.* **2007**, *93*, 2373.

(21) Estrela-Lopis, I.; Brezesinski, G.; Möhwald, H. *Chem. Phys. Lipids* **2004**, *131*, 71.

(22) Helm, C. A.; Möhwald, H.; Kjaer, K.; Als-Nielsen, J. *Europhys. Lett.* **1987**, *4*, 697.

(23) *Handbook of Chemistry and Physics*, 67 ed.; CRC-press: Cleveland, OH, 1986-87.

(24) Miller, A.; Möhwald, H. *J. Chem. Phys.* **1987**, *86*, 4258.

(25) Tsukanova, V.; Grainger, D.; C. Salesse . Langmuir, 5539-5550. *Langmuir* **2002**, *18*, 5539.

(26) Schmitt, J.; Mächtle, P.; Eck, D.; Möhwald, H.; Helm, C. A. *Langmuir* **1999**, *15*, 3256.

(27) Thoma, M.; Schwendler, M.; Baltes, H.; Helm, C. A.; Pfohl, T.; Riegler, H.; Möhwald, H. *Langmuir* **1996**, *12*, 1722.

(28) Brezesinski, G.; Thoma, M.; Struth, B.; Möhwald, H. *J. Phys. Chem.* **1996**, *100*, 3126.

TOC Image